To cite this article: YU J W, YAO C B, ZHANG Z G, et al. Numerical prediction method of shafting power characteristics of free self-propelled ship in waves[J/OL]. Chinese Journal of Ship Research, 2022, 17(3). http://www.ship-research.com/en/article/doi/10.19693/j.issn.1673-3185.02733.

DOI: 10.19693/j.issn.1673-3185. 02733

Numerical prediction method of shafting power characteristics of free self-propelled ship in waves

YU Jiawei[1,2], *YAO Chaobang*[*1,2], *ZHANG Zhiguo*[1,2], *FENG Dakui*[1,2], *WANG Xianzhou*[1,2]

1 School of Naval Architecture and Ocean Engineering, Huazhong University of Science and Technology, Wuhan 430074, China

2 Key Laboratory of Ship and Ocean Hydrodynamics of Hubei Province, Huazhong University of Science and Technology, Wuhan 430074, China

Abstract: [**Objective**] To investigate ship power characteristics and the difference between the towing model and self-propulsion model for ship motion response in waves, numerical simulations of ship self-propulsion performance in waves are carried out. [**Methods**] In this paper, the KCS ship model and KP505 propeller model are selected, and the unsteady Reynolds-averaged Navier-Stokes (URANS) method is used to carry out computational fluid dynamics (CFD) simulations of ship self-propulsion in waves. The in-house URANS solver HUST-Ship and in-house structured dynamic overset grid code HUST-Overset are combined to solve the motions of the self-propelled ship in waves, and the improved body-force model is selected as the propulsion model. Towing simulations for KCS with two degrees of freedom (2-DOFs) in waves and self-propulsion simulations with 3-DOFs under different wave conditions are carried out, and the differences between these methods are discussed in detail. Finally, the components and their specific proportions of added power during ship self-propulsion in waves are analyzed in detail using the logarithmic analysis method. [**Results**] Regarding the added power of a self-propelled KCS in waves, the added resistance is responsible for 74%−77% while propulsive efficiency accounts for 23%−26%, that is, the added resistance occupies a larger proportion. [**Conclusion**] Reducing ship motion to decrease added resistance is the most effective approach to reducing added power.

Key words: self-propelled in waves; shafting power characteristics; improved body-force model; dynamic overset grid

CLC number: U661.32^{+}2

0 Introduction

Conventional ship design focuses on the impacts of ship resistance and self-propulsion performance on the speed and economy of ships in still water [1]. However, a ship inevitably undergoes marked motion in real voyages due to environmental factors such as wind, waves, and currents. The consequent wave-added resistance and stalling further affect the ships' economy. Therefore, evaluating and optimizing the kinematics and seaworthiness of self-propelled ships in waves, not just in still water, is

Received: 2021 − 12 − 30 **Accepted:** 2022 − 02 − 20

Supported by: National Natural Science Foundation of China (52071148); Joint Funds of the National Natural Science Foundation of China and Chi-Sun Yeh Science Foundation (U2141228); Fundamental Research Funds for the Central Universities (2021JYCXJJ038)

Authors: YU Jiawei, male, born in 1996, Ph.D. Research interests: prediction of ship hydrodynamic performance, novel propulsion numerical models, and viscous potential flow coupling. E-mail:yu_jiaw@hust.edu.cn

YAO Chaobang, male, born in 1987, Ph.D., associate professor. Research interests: the theory of ship motion in waves, multi-ship/multi-floating body hydrodynamic interference, ship maneuverability in still water and waves, and viscous potential flow coupling methods. E-mail:yaochaobang@hust.edu.cn

ZHANG Zhiguo, male, born in 1962, Ph.D., professor. Research interests: computational ship hydrodynamics and ship hydrodynamic performance. E-mail:zzg@hust.edu.cn

***Corresponding author:** YAO Chaobang

crucial for ships' safety and economy.

At present, three major methods to predict ships' seakeeping performance are available, i. e., model test, potential-flow theory, and computational fluid dynamics (CFD) viscosity simulation. Experimental fluid dynamics (EFD) is able to provide the most reliable data and uncertainty analysis results for CFD verification, and it is still irreplaceable for the time being, despite its long cycle and high costs. In recent years, CFD has gradually been regarded as an effective method of predicting and evaluating ships' seakeeping performance due to its advantages of high fidelity, low cost, and high precision. Simonsen et al. [2] used EFD and CFD to study the performance of a standard ship model of the container ship of the Korea Research Institute of Ships and Ocean Engineering (KRISO Container Ship, abbreviated as KCS) in still water and regular head waves. They also carried out CFD simulation with the unsteady Reynolds-averaged Navier-Stokes (URANS) software, namely, CFDSHIP-IOWA and STAR-CCM+ , and the potential-flow program AEGIR. The uncertainty analysis and evaluation based on EFD data show that the level of uncertainty is comparable to that of the planar motion mechanism (PMM) in still water but is higher than that of the PMM in waves. Compared with the potential-flow results, the motion and average resistance results obtained with URANS software are closer to measured data. Wei et al. [3] employed the URANS method to investigate the navigation performance of monohull, twin-hull, and trimaran new-concept high-speed shuttle vessels in waves. Resorting to STAR-CCM+, Zhang et al. [4] studied the seakeeping performance of a small-waterplane-area trimaran ship and found that the seakeeping performance of the boat became better when its side hull was close to the bow. Jin et al. [5] adopted STAR-CCM+ to predict the hydrodynamic characteristics of two liquefied natural gas (LNG) carriers in regular head and oblique waves and studied the load on ships and the ships' motion under different wave conditions by evaluating the numerical uncertainty through uncertainty analysis. Their calculation results are in excellent agreement with the result given by the EFD and that predicted by the potential-flow program.

In addition to the wave environment, the rotating propeller also induces a ship to be affected by dynamic factors, including time-varying wake flow distribution, propulsion factors, ship motion, stalling, and reserve power. With the development of ship design, studying the influence of propeller load fluctuations on ships' navigation performance in waves is of great significance because the power and the rotational speed of the engine undergo huge fluctuations under this operating condition. Wang et al. [6] studied the motion response and stalling of the standard self-propelled ship model, the Office of Naval Research Tumblehome (ONRT), in regular head waves by combining CFD with dynamic overset grid technology. The agreement between CFD and EFD results indicates that the method is suitable for self-propulsion prediction in waves. Lee et al. [7] predicted the power gain/speed loss and the propulsion performance of the KVLCC2 ship model by integrating URANS with the finite volume method (FVM) and the volume of fluid (VOF) model. Then, simulation calculations of towing and self-propulsion in still water and waves were conducted to forecast the self-propulsion factor, resistance, and wave-added resistance. Moreover, they investigated the speed-power relationship and propulsion performance in waves by four methods, including the Taylor expansion method, the direct dynamic method, the load variation approach, and the constant thrust method.

In summary, the present studies of ships' seakeeping performance primarily focus on the test and simulation of constrained models. However, research results on the influence of the propeller on the ship motion characteristics of self-propelled models, as well as those on the reserve power or stalling in waves and propulsion performance of self-propelled models, are scarce. For this reason, CFD simulation of free direct navigation in waves will be conducted by the URANS method on the basis of the KCS ship model and the KP505 propeller model in this study; the self-propelled motion of a ship in waves will be solved by coupling the self-developed URANS solver, HUST-Ship, and the self-developed structured dynamic overset grid code, HUST-Overset; moreover, an improved body-force propeller propulsion model based on the hybrid blade element-momentum method will be chosen to ensure a proper balance among prediction accuracy, prediction reliability, and computational efficiency [8-10]. Specifically, the motion response characteristics and the wave-added resistance in the case of the constrained KCS model with two degrees of freedom (2-DoFs) (heave and pitch) in waves are studied, and the reliability of numerical

calculation in waves is verified by experimental data. Next, an improved body-force method is employed to simulate the direct navigation of the KCS self-propelled model with 3-DoFs (heave, pitch, and surge) under different wave conditions. The aim is to study the motion response characteristics, reserve power, and propulsion efficiency of the KCS in a free direct navigation state in waves, thereby comparing and analyzing the differences in motion characteristics between the constrained model and the self-propelled model of ships under the same frequency of encounter. Eventually, the major factors affecting the power gain of a ship in waves and their specific proportions are analyzed by a logarithmic analysis method to provide a reference for the numerical prediction of the shafting power characteristics of free self-propelled ships in waves.

1 Numerical methods

1.1 Governing equations and improved body-force model

In this paper, the self-developed CFD solver, HUST-Ship, will be used for the CFD simulations of towing and self-propulsion in still water and waves. The reliability of HUST-Ship has been verified [8-12] by the simulations of various propellers, ships, and underwater vehicles in still water and waves. The Reynolds-averaged Navier-Stokes (RANS) governing equations can be obtained by averaging the continuity equation and the momentum conservation equation over time:

$$\frac{\partial u_i}{\partial x_i} = 0 \tag{1}$$

$$\frac{\partial u_i}{\partial t} + u_j \frac{\partial u_i}{\partial x_j} = -\frac{1}{\rho}\frac{\partial p'}{\partial x_i} + \frac{1}{\rho}\frac{\partial}{\partial x_j}\left(\mu \frac{\partial u_i}{\partial x_j} - \rho \overline{u_i' u_j'}\right) + f_{\mathrm{bi}} \tag{2}$$

where u_i and u_j (i, j = 1, 2, 3) are the time-averaged components of the velocity vector in the three directions of the 3D Cartesian coordinate system; x_i and x_j are the velocity component-based coordinates in the three directions; t is time; ρ is density; p' is the dynamic fluid pressure; μ is the dynamic viscosity coefficient of fluid; $-\rho\overline{u_i' u_j'}$ is Reynolds stress; f_{bi} is the force on the unit volume of the propeller.

In addition, the two-equation eddy-viscosity k-ω model is chosen to serve as the turbulence model in this paper [13].

The so-called body-force method is to add a simplified cylindrical area at the stern of a ship to replace the propeller and add a body-force term f_{bi} to the right end of the momentum equation to generate the corresponding force and moment for the propeller. In this paper, an improved body-force model, the modified Osaka University method (MOUM) [6], will be employed. This is a blade element-momentum theory (BEMT) considering the viscous effect of a 3D propeller, and it takes the instantaneous speed at the propeller disk at the current time as the advance speed of the propeller during iterative calculation.

1.2 Free surface capturing

In this paper, the single-phase Level-set method will be employed in the simulation to capture the change in the free surface. In ship and marine engineering studies, the mutual transformation between the water phase and the gas phase is generally not considered, that is, no mass conversion at the two-phase flow interface, and the density and the viscosity of air are much smaller than those of water. Therefore, the impacts of air density and viscosity can be ignored in simulation so that the single-phase Level-set method can be employed for solving. The distance between an arbitrary point in the flow field and the free surface is defined as ϕ, and the free surface can then be expressed as $\phi = 0$. The Level-set equation is expressed as [14]

$$\frac{\partial \phi}{\partial t} + \boldsymbol{v}\nabla\phi = 0 \tag{3}$$

where $\boldsymbol{v}$ is the velocity vector. $\phi = 0$ represents the free surface, $\phi > 0$ and $\phi < 0$ indicate the cases in air and in water, respectively.

1.3 Wave-making and wave-eliminating methods

In the HUST-Ship solver, the velocity boundary wave-making method [15] will be utilized to generate target waves. When the target waves to be simulated exhibit a wavelength of λ and a wave height of A, the change $l(t)$ in the free surface at the entrance is

$$l(t) = A\cos(kx_1 - \omega t + \varphi) \tag{4}$$

The corresponding velocity components on the velocity boundary are

$$u_1 = A\omega \frac{\cosh k(x_3 + d)}{\sinh kd}\cos(kx_1 - \omega t + \varphi) \tag{5}$$

$$u_3 = A\omega \frac{\sinh k(x_3 + d)}{\sinh kd}\sin(kx_1 - \omega t + \varphi) \tag{6}$$

where A, k, ω, and φ are the amplitude, wavenumber, circular frequency, and initial phase of the subcomponent regular waves, respectively; d is the water depth; x_1/x_3 and u_1/u_3 are the coordinates and velocity in the first/third coordinate direction, respectively. To reduce the impact of wave reflection on

the simulation results in the course of wave elimination, this paper will employ two methods, namely grid attenuation and momentum-based wave elimination.

1.4 PI speed controller

In self-propulsion control, the proportional integral (PI) speed controller is a method to directly match the propeller's rotational speed by free direct navigation [16], and its principle is to control ship speed with the PI regulator to meet the set value, i.e.,

$$n = Pe + I\int e\mathrm{d}t \tag{7}$$

where n is the propeller's rotational speed; P is the proportional coefficient; $e = u_{\mathrm{tar}} - u_{\mathrm{ship}}$ is the difference between the target speed u_{tar} and the actual ship speed u_{ship}; I is the integral coefficient.

In the self-developed software HUST-Ship, the values of P and I will be given at the initial moment of calculation. Then, they vary with each calculation time step until the target speed is reached and force balance in the direction of the ship's length is achieved. The rotational speed matching under the self-propulsion point is now completed.

2 Operating conditions and grids

2.1 Operating conditions in simulation

The ship model and the propeller model simulated in this paper are KCS with rudder and the KP505 propeller, respectively, and the scale ratio is 1:37.89. The experimental data on the open water, resistance, self-propulsion, and head-wave motion response of the model are all from the Tokyo 2015 workshop [17]. According to the experimental operating conditions of the Tokyo 2015 workshop, the CFD simulation conditions (2-DoFs) are set as shown in Table 1. In the table, L_{pp} is the length between the perpendiculars of the ship; the ship speed corresponding to the Froude number F_r = 0.26, as well as the rotational speed of self-propulsion in waves, can be matched by the PI speed controller.

2.2 Structured overset grids

In this paper, structured dynamic overset grids will be used and processed by the self-developed overset grid program HUST-Overset. This program is grid-point oversetting of structured grids and involves three steps, namely, digging holes, finding points, and identifying contributory units. Specifically, holes are dug by a hole mapping method based on uniform Cartesian coordinate grids; then, the data structure based on the alternating digital tree (ADT) is taken to find contributory units for the interpolation points, and the relationships of the contributory units with the interpolation points can be obtained by tri-linear interpolation [18-19].

Table 1 Parameter setting for operating conditions in CFD simulation

Number of operating condition in simulation	Wavelength λ/L_{pp}	Wave height A/L_{pp}	Propulsion model
1	Still water	Still water	w/o
2	0.65	0.0108	
3	0.85	0.0142	
4	1.15	0.0192	
5	1.95	0.0325	
6	0.65	0.0108	MOUM
7	0.85	0.0142	
8	1.15	0.0192	
9	1.95	0.0325	

Overset grid technology is able to decompose a complex object into several simple parts, divide grids on each part separately, and then embed the grids on each part into the background grids. For example, regarding the complex KCS surface in this study, grid division can be conducted separately on the main hull, the stern, and the rudder, and the grids are then spliced into the whole-ship grids, as shown in Fig. 1. When multiple sets of mutually-unrelated grids cover the entire computational domain, overlapping parts occur among the various sets of grids. In this case, the grids outside the computational domain shall be dug out by hole digging, and an interpolation relationship can then be built for the remaining grids in the overlapping areas. Therefore, data can be exchanged among the various sets of grids through overlapping areas, thereby solving the entire computational domain; As a result, overset grids exhibit the advantages of high efficiency in grid generation, strong wall simulation ability, and effectiveness in dealing with complex spatial geometric models. To capture the fine flows around the hull and the propeller, the grids shown in Fig. 1 are densified significantly. Free densification according to specific needs is also an advantage of overset grids.

3 Analysis of simulation results

3.1 Simulation of towing in waves

Specifically, the constrained KCS model was simulated in regular head waves according to the test

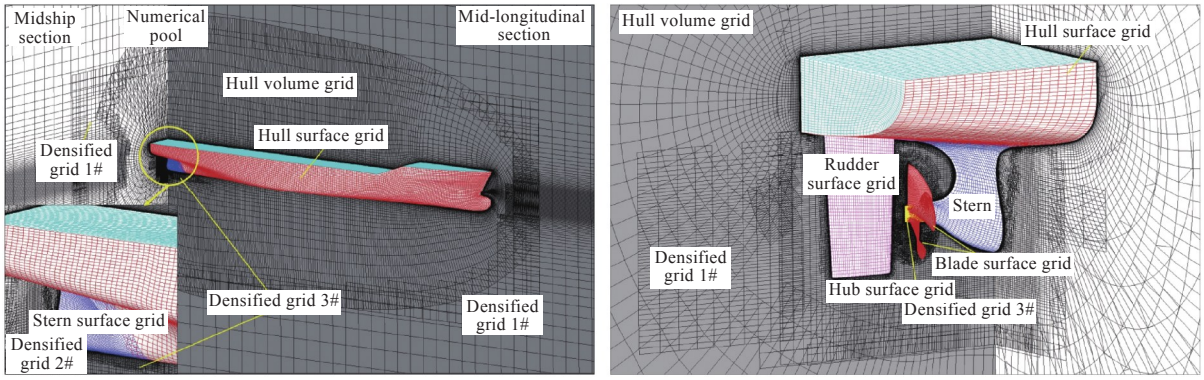

(a) Surface grids and volume grids on main body of hull (b) Detailed surface grids and volume grids on stern

Fig. 1 Structured overset grids in operating condition of self-propulsion with discrete propeller

conditions provided by the Tokyo 2015 workshop [15], with the results shown in Fig. 2. Two DoFs, heave and pitch, were released in the simulation; the wavelength of regular waves falls within $0.65L_{pp}$–$1.95L_{pp}$; the steepness is a constant value (A/λ = 1/60). Fig. 2 compares the time-history curve of wave height at $x_1 = 0$ obtained by CFD simulation with the curve of the EFD theoretical value under four wave conditions. Visibly, the two are almost identical.

Then, according to the uncertainty protocols recommended by the international towing tank conference (ITTC), uncertainty analysis of resistance coefficient C_T, heave transfer function TF_3, and pitch transfer function TF_5 under the condition of a wavelength of $1.95L_{pp}$ was performed. The results of uncertainty analysis under different grids and different time steps are shown in Table 2, and the verification results based on the experimental data are reported in Table 3. In the two tables, r_G and r_T are the respective refinement rate for the grid and the time step; $S_{G1}/S_{G2}/S_{G3}$ and $S_{T1}/S_{T2}/S_{T3}$ are the uncertainty analysis results for sparse/medium/dense grids and the sparse/medium/dense time step, respectively; U_G and U_T are the uncertainty of the grids and the time step, respectively; U_{SN} is the numerical uncer-

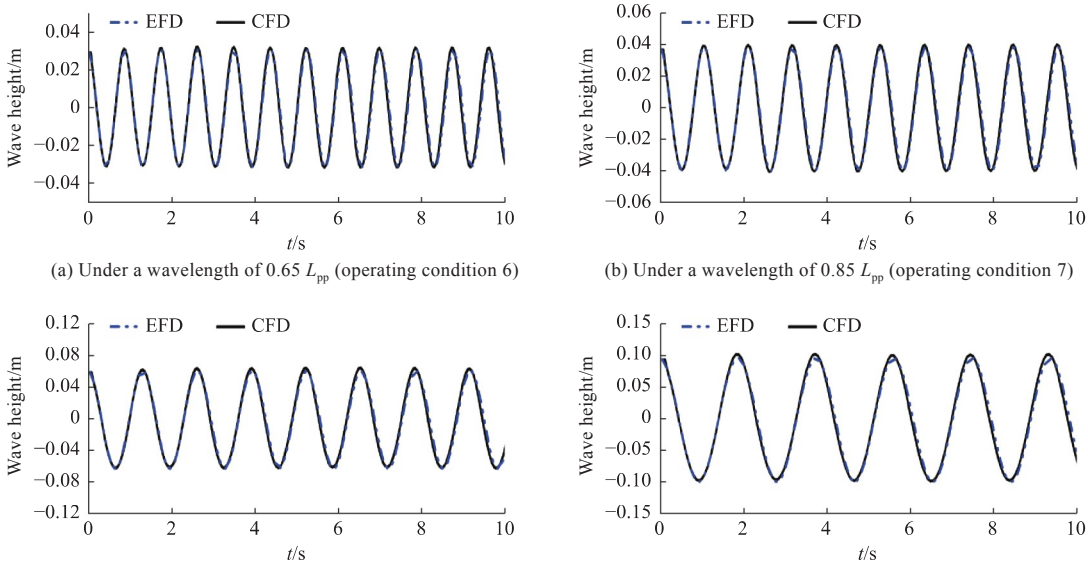

(a) Under a wavelength of 0.65 L_{pp} (operating condition 6) (b) Under a wavelength of 0.85 L_{pp} (operating condition 7)

(c) Under a wavelength of 1.15 L_{pp} (operating condition 8) (d) Under a wavelength of 1.95 L_{pp} (operating condition 9)

Fig. 2 Comparison between simulation results and theoretical results of regular wave

Table 2 Results of uncertainty analysis under different grids and time steps

	r_G	Results			(U_G/D)/%	r_T	Results			(U_T/D)/%
		S_{G1}	S_{G2}	S_{G3}			S_{T1}	S_{T2}	S_{T3}	
C_T		10.542	11.811	11.999	4.04		10.552	11.811	11.914	0.29
TF_3	$\sqrt{2}$	0.922	0.935	0.938	1.12	2	0.920	0.935	0.942	1.42
TF_5		1.136	1.111	1.107	0.95		1.131	1.111	1.103	1.20

tainty; U_D is the experimental uncertainty; U_V is the verification uncertainty; D is the experimental data. The analysis results show that the comparison errors E are all smaller than the verification uncertainty U_V, which means that the numerical calculation results are verified at the U_V level. Under this wave condition, the error between the motion response predicted by simulation and the experimental result is not larger than 1%. Fig. 3 shows the simulation and experimental curves of heave and pitch motion responses. Evidently, the simulation errors are all below 5%, indicating that HUST-Ship can accurately predict the motion of ships in waves.

Table 3 Validation results based on test data

	(U_G / D) /%	(U_T / D) /%	(U_{SN} / D) /%	(U_D / D) /%	(U_V / D) /%	(E / D) /%
C_T	4.04	0.29	4.33	8	9.10	8.94
TF_3	1.12	1.42	2.54	4	4.74	0.37
TF_5	0.95	1.20	2.15	4	4.54	0.65

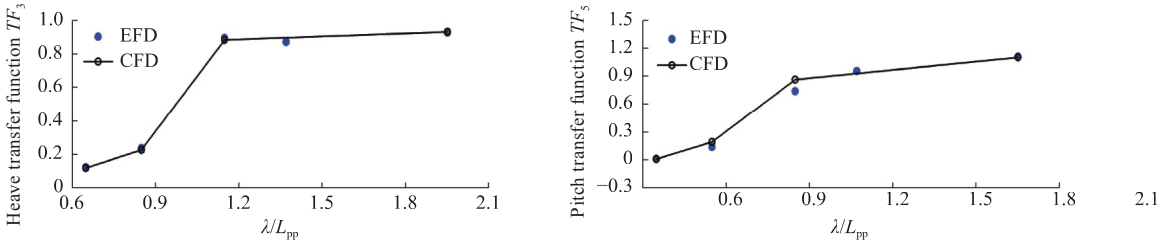

(a) Heave response curves (b) Pitch response curves

Fig. 3 Simulation curves and test curves of heave and pitch motion responses

3.2 Simulation of self-propulsion in waves

This section presents the simulation of self-propulsion in waves under four wave conditions. In particular, the self-propelled model releases three DoFs, i.e., heave, pitch, and surge, takes the target speed of 2.017 m/s as the control object, and adopts the PI control method to match the propeller's rotational speed corresponding to the target speed. Fig. 4 shows the time-history curves of the propeller's rotational speed and those of the relative ship speed of the KCS ship model in the course of self-propulsion in head waves simulated under different wave conditions.

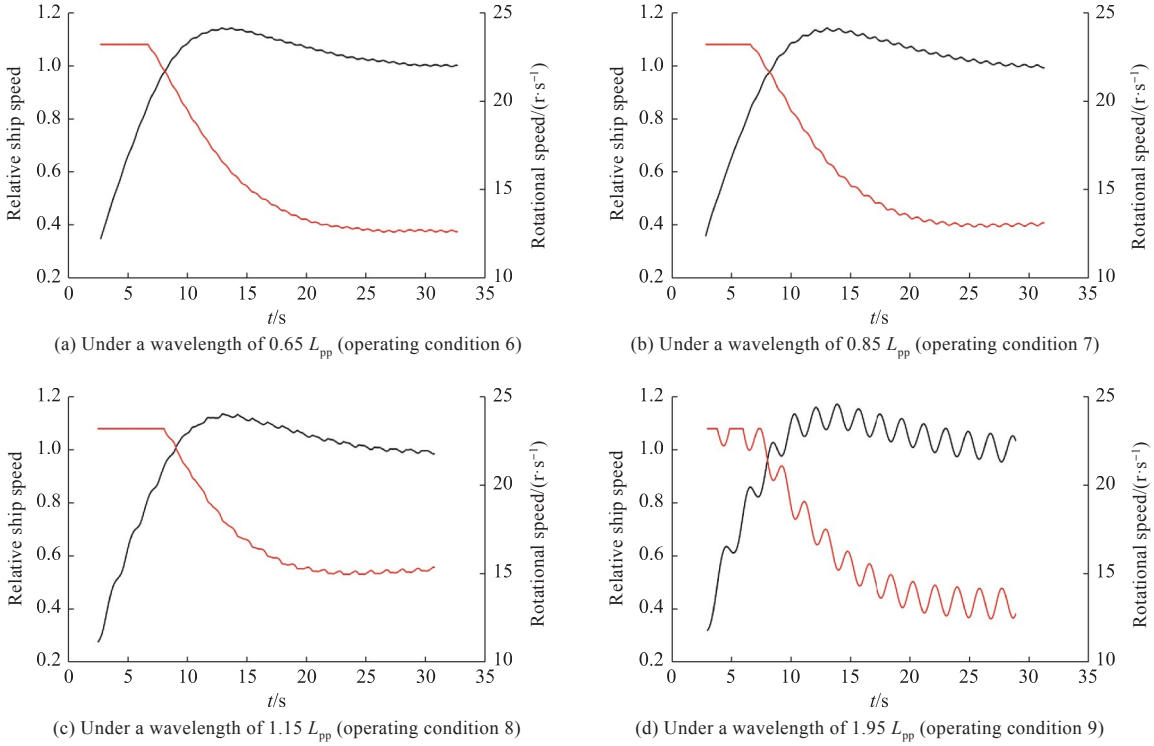

(a) Under a wavelength of 0.65 L_{pp} (operating condition 6)

(b) Under a wavelength of 0.85 L_{pp} (operating condition 7)

(c) Under a wavelength of 1.15 L_{pp} (operating condition 8)

(d) Under a wavelength of 1.95 L_{pp} (operating condition 9)

Fig. 4 Curve of propeller's rotational speed and ship speed curve of KCS ship model in self-propulsion under different wave conditions

Fig. 5 compares the motion response curves of the two different simulation methods, namely, the self-propelled model and the restrained model in waves. Clearly, compared with the restrained model, the self-propelled KCS model provides smaller values of the transfer functions for the ship motion responses in head waves. Nevertheless, the deviations are below 5%. Hence, the influence of the propeller on the ship's motion amplitude is insignificant. The above results verify the rationality of towing tests in predicting the motion responses of self-propelled ships in waves.

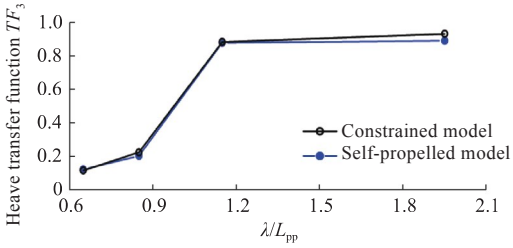

(a) Heave response curves

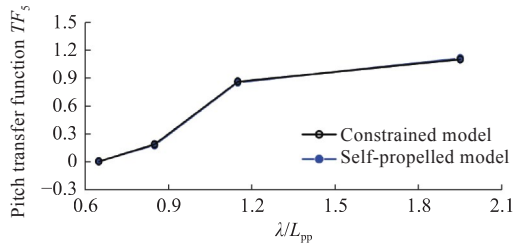

(b) Pitch response curves

Fig. 5 Heave and pitch response curves of self-propelled and constrained models in waves

The simulation results of wave-added resistance and self-propulsion in waves are presented in Table 4, where ΔR is the wave-added resistance and Q is the propeller torque.

Table 4 Simulation results of wave-added resistance and self-propulsion in waves

λ/L_{pp}	ΔR/N	Q/(N·m)	n/（r·s^{-1}）
Still water	0	2.049	12.021
0.651	2.129	2.325	12.754
0.851	10.8	2.41	13.092
1.15	45.556	3.474	15.227
1.951	15.905	2.555	13.475

For a detailed analysis of the factors affecting the power gain of a ship in waves and their proportions, the logarithmic analysis method [20] will be employed in this paper to analyze the ship's propulsion efficiency $\eta = Ru/2\pi nQ$, that is, to quantify the contribution percentages of wave-added resistance R, ship speed u, and propulsion efficiency η to the reserve power of self-propulsion in waves, $2\pi nQ$. The details are as follows

$$\Delta(\lg\eta) = \frac{\Delta\eta}{\eta} = \frac{R_w - R_{cw}}{R_{cw}} + \frac{u_w - u_{cw}}{u_{cw}} + \frac{(nQ)_w - (nQ)_{cw}}{(nQ)_{cw}} \tag{8}$$

where subscripts w and cw stand for the operating conditions of waves and still water, respectively. Since ship speed is taken as the control object of the simulation, the average end-state ship speed is $u_w = u_{cw}$.

A comprehensive consideration of Eq. (7) and the simulation results in Table 4 indicates that the power gain of the KCS ship model during self-propulsion in waves is primarily caused by two factors, propulsion efficiency and wave-added resistance. In particular, their contributions to the power gain account for 23%−26% and 74%−77%, respectively. In other words, the reserve power is mainly caused by wave-added resistance, which is in turn largely induced by ship motion. Therefore, reducing wave-added resistance by mitigating ship motion is the most effective means to lower the power gain in waves.

4 Conclusions

In this paper, on the basis of the KCS ship model and the KP505 propeller model, the self-propelled motion of a ship in waves was solved by coupling the self-developed URANS solver HUST-Ship with the self-developed structured dynamic overset grid code HUST-Overset. In addition, the URANS method was used for the CFD simulation of a ship's free direct navigation in waves. The following conclusions were drawn.

1) The comparison between the CFD results and the EFD data verifies the reliability of coupling HUST-Ship with the overset grid code HUST-Overset to solve the motion responses of a ship in waves.

2) According to the results of motion responses in waves simulated by the self-propelled model and the restrained model, the self-propelled model provides smaller transfer function values for the ship's motion responses. Nevertheless, the deviation is lower than 5%. Therefore, the propeller has a minor impact on the ship's motion responses, and the rationality of conducting towing tests to predict the motion responses of a self-propelled ship in waves is

thereby verified.

3) The power gain of a ship in waves is mainly caused by two factors, propulsion efficiency and wave-added resistance, and the contribution of the latter is larger.

References

[1] ZHANG L, ZHANG J N, SHANG Y C. A practical direct URANS CFD approach for the speed loss and propulsion performance evaluation in short-crested irregular head waves [J]. Ocean Engineering, 2021, 219: 108287.

[2] SIMONSEN C D, OTZEN J F, JONCQUEZ S, et al. EFD and CFD for KCS heaving and pitching in regular head waves [J]. Journal of Marine Science and Technology, 2013, 18 (4): 435−459.

[3] WEI C Z, YI H, LI Y H. Hull forms and straight forward CFD free running trials of high-speed shuttle vessels [J]. Chinese Journal of Ship Research, 2017, 12 (2): 12−21 (in Chinese).

[4] ZHANG M X, LU P C, WANG Z H. Numerical simulation of seakeeping performance of a trimaran small waterplane area center hull [J]. Chinese Journal of Ship Research, 2020, 15 (4): 135−143, 152 (in Chinese).

[5] JIN Y T, CHAI S H, DUFFY J, et al. URANS predictions of wave induced loads and motions on ships in regular head and oblique waves at zero forward speed [J]. Journal of Fluids and Structures, 2017, 74: 178−204.

[6] WANG J H, WAN D C. Numerical investigations of free running ship in bow quartering waves under course keeping control [J]. Chinese Journal of Hydrodynamics, 2018, 33 (6): 740−748 (in Chinese).

[7] LEE C M, SEO J H, YU J W, et al. Comparative study of prediction methods of power increase and propulsive performances in regular head short waves of KVLCC2using CFD [J]. International Journal of Naval Architecture and Ocean Engineering, 2019, 11 (2): 883−898.

[8] FENG D K, YU J W, HE R, et al. Improved body force propulsion model for ship propeller simulation [J]. Applied Ocean Research, 2020, 104: 102328.

[9] FENG D K, YU J W, HE R, et al. Free running computations of KCS with different propulsion models [J]. Ocean Engineering, 2020, 214: 107563.

[10] YU J W, YAO C B, LIU L W, et al. Assessment of full-scale KCS free running simulation with body-force models [J]. Ocean Engineering, 2021, 237: 109570.

[11] ZHANG Z G, GUO L X, WEI P, et al. Numerical simulation of submarine surfacing motion in regular waves [J]. Iranian Journal of Science and Technology, Transactions of Mechanical Engineering, 2020, 44 (2): 359−372.

[12] LIU L W, CHEN M X, YU J W, et al. Full-scale simulation of self-propulsion for a free-running submarine [J]. Physics of Fluids, 2021, 33 (4): 047103.

[13] MENTER F R. Two-equation eddy-viscosity turbulence models for engineering applications [J]. AIAA Journal, 1994, 32 (8): 1598−1605.

[14] BURG C O E. Single-phase level set simulations for unstructured incompressible flows [C]//17th AIAA Computational Fluid Dynamics Conference. Toronto, Canada: American Institute of Aeronautics and Astronautics Inc., 2005.

[15] FENG D K, LU J J, WEI P, et al. The research of wave-generating in 3-D numerical wave tank based on level-set method [J]. Chinese Journal of Hydrodynamics, 2018, 33 (4): 435−444 (in Chinese).

[16] CARRICA P M, CASTRO A M, STERN F. Selfpropulsion computations using a speed controller and a discretized propeller with dynamic overset grids [J]. Journal of Marine Science and Technology, 2010, 15 (4): 316−330.

[17] Tokyo 2015. A workshop on CFD in ship hydrodynamics [DB/OL]. (2015-12-2) [2021-12-30]. https://t2015.nmri.go.jp/index.html.

[18] LI T H, YAN C. Investigation of automatic generation technique for two-dimensional DRAGON grid [J]. Acta Aerodynamica Sinica, 2005, 23 (1): 88−92 (in Chinese).

[19] LI T H. Investigation of chimera grid automatic generation algorithm [D]. Beijing: Beihang University, 2004 (in Chinese).

[20] SANADA Y, KIM D H, SADAT-HOSSEINI H, et al. Assessment of experimental and CFD capability for KCS added power in head and oblique waves [C]// 33rd Symposium on Naval Hydrodynamics. Osaka, Japan:[s.n.], 2020.

波浪中自由自航船舶轴系功率特性的数值预报方法

余嘉威[1,2],姚朝帮*[1,2],张志国[1,2],冯大奎[1,2],王先洲[1,2]

1 华中科技大学 船舶与海洋工程学院,湖北 武汉 430074

2 华中科技大学 船舶和海洋水动力湖北省重点实验室,湖北 武汉 430074

摘　要:[**目的**]为了研究船舶在波浪中约束模与自航模运动特性的差异以及船舶轴系功率特性,开展船舶波浪中自航性能数值仿真预报。[**方法**]首先,选取KCS船模和KP505桨模,采用URANS方法进行船舶波浪自由直航CFD模拟;然后,基于自研URANS求解器HUST-Ship与自研结构化动态重叠网格代码HUSTOverset,以及改进型体积力螺旋桨推进模型,对船舶在不同波浪条件下的运动响应进行耦合求解,包括两自由度KCS约束模运动仿真和三自由度自航模自由直航仿真,并对比这2种方法预报船舶运动特性的差异;最后,采用对数分析法得出波浪中船舶自由直航功率增加的主要成分及其具体占比。[**结果**]KCS船模在波浪中自航时,推进效率和波浪增阻对功率增加的贡献占比分别为23%~26%和74%~77%,即波浪增阻占比较大。[**结论**]因此,降低波浪中功率增加的最有效方法是减小船舶运动以降低波浪增阻。

关键词:波浪自航;轴系功率特性;改进型体积力模型;结构化动态重叠网格